Available online at www.sciencedirect.com
SCIENCE DIRECT®
Journal of Sound and Vibration 264 (2003) 245–251
JOURNAL OF SOUND AND VIBRATION
www.elsevier.com/locate/jsvi

Letter to the Editor

The Saint-Venant principle and an impact load acting on an elastic half-space

J. Awrejcewicz*, Yu. Pyryev

Department of Automatics and Biomechanics, Technical University of Lodz, Stefanowskiego 1/15, Lodz 90-924, Poland

Received 12 July 2002; accepted 23 October 2002

1. Introduction

In this letter two following questions are addressed: Is it possible to use the Saint-Venant principle in the elastodynamic problems of impact loads acting onto an elastic half-space, and under which conditions? Note that, in general, the Saint-Venant principle may be briefly described in the following way: if a given system of forces acting on a small area of an elastic body surface is substituted by another statically equivalent forces system then this change introduces only local variations of the stress–strain state, and the differences between two corresponding stress–strain states might be negligible sufficiently far from the forces place action [1,2].

In order to give an answer to the above formulated questions, the classical axially symmetric Lamb's problem is considered. The response of a semi-infinite elastic solid to a pulsed concentrated force is referred to as "Lamb's problem". Following Lamb's classic paper [3] this problem has been investigated by many authors (see Refs. [4–7] and citations therein).

It is assumed that an impacting load of the unit jump-type possesses the different distribution on a circle of an elastic half-space. The stress–strain state is defined applying the Hankel and Laplace transformations, and then the inversed transformations are found numerically.

2. Mathematical formulation of the problem

Let the plane $z = 0$ being the boundary of an elastic half-space is subjected to an axially symmetric impact excitation (load) of the jump type along the z-axis. In the considered half-space, the strain–stress state is excited, and the longitudinal (dilatation), shear (distortion) and surface Rayleigh types of wave pulses are born.

*Corresponding author. Tel.: +48-42-6312378; fax: +48-42-6312225.
E-mail address: awrejcew@ck-sg.p.lodz.pl (J. Awrejcewicz).

0022-460X/03/$ - see front matter
doi:10.1016/S0022-460X(02)01473-6

The problem is reduced to find the solutions of two linear dynamical equations (in cylindrical co-ordinates) of the form

$$(\lambda+2\mu)\left(\frac{\partial^2 u}{\partial r^2}+\frac{1}{r}\frac{\partial u}{\partial r}-\frac{u}{r^2}\right)+\mu\frac{\partial^2 u}{\partial z^2}+(\lambda+\mu)\frac{\partial^2 w}{\partial r\partial z}=\rho\frac{\partial^2 u}{\partial t^2}, \tag{1}$$

$$(\lambda+\mu)\left(\frac{\partial^2 u}{\partial r\partial z}+\frac{1}{r}\frac{\partial u}{\partial z}\right)+\mu\left(\frac{\partial^2 w}{\partial r^2}+\frac{1}{r}\frac{\partial w}{\partial r}\right)+(\lambda+2\mu)\frac{\partial^2 w}{\partial z^2}=\rho\frac{\partial^2 w}{\partial t^2} \tag{2}$$

with the attached boundary

$$\sigma_{zz}=-Z(r)f(t),\quad \sigma_{zr}=0\quad \text{for } z=0,\quad u,w\to 0\quad \text{for } z\to\infty \tag{3}$$

and initial conditions

$$u=\partial u/\partial t=w=\partial w/\partial t=0 \text{ for } t<0 \tag{4}$$

where: λ, μ are the Lamé constants, ρ is the density, $u(r,z)$, $w(r,z)$ are the displacement components in direction of the axes r and z, respectively.

Furthermore, σ_{rr} σ_{zz}, and $\sigma_{\theta\theta}$ are the normal components in cylindrical co-ordinates, σ_{zr} is the tangential component of the stress, and $\mathrm{H}(t)=1,\ t>0$; $\mathrm{H}(t)=0,\ t<0$.

It is assumed that a variation of $f(t)$ in time is of the unit jump type

$$f(t)=\mathrm{H}(t),\ \ \tilde{f}(s)=\mathscr{L}[\mathrm{H}(t)]=\int_0^\infty \mathrm{H}(t)\mathrm{e}^{-st}\mathrm{d}t=1/s$$

where $\mathscr{L}$ denotes the Laplace transform, and that the load variations on the surface are governed by the following formulae:

$$Z(r)=\frac{P}{\pi r_0^2}\mathrm{H}(r_0-r),$$

$$\bar{Z}(k)=\mathrm{H}[Z(r)]=\int_0^\infty Z(r)\mathrm{J}_0(kr)r\mathrm{d}r=\int_0^{r_0} Z(r)\mathrm{J}_0(kr)r\mathrm{d}r=\frac{P}{2\pi}\left(2\frac{\mathrm{J}_1(kr_0)}{kr_0}\right),$$

where H is the Hankel transform and $\mathrm{J}_n(x)$ is a Bessel function of the first kind of order n ($n=0,1,2,\ldots$).

Although the radius of the surface load action r_0 may change and even may approach zero (concentrated force), but always the following relation holds: $\lim_{r_0\to 0,\ Z\to\infty} Z(r)\pi r_0^2=P$. The Hankel transformation of a force yields $\bar{Z}(k)=P/2\pi$.

3. Solution of the problem

Applying the Laplace and Hankel transformations to Eqs. (1) and (2), and taking into account the homogeneous initial conditions (4) yield linear differential equations with respect to the unknown z. Since a solution of these equations depends on four unknowns, they are found using four boundary conditions (3). Applying the inverse Laplace and Hankel transformations, and

introducing the new integration variables ($r > 0$), the following relations are obtained:

$$2\pi\mu r_0 w(r,\, z,\, t)/P = \frac{1}{\xi}\int_0^{\infty}\left(\frac{1}{2\pi \mathrm{i}}\int_{c_0-\mathrm{i}\infty}^{c_0+\mathrm{i}\infty} w_0^{LH}\frac{\mathrm{e}^{\tau y}}{y}\mathrm{d}y\right)\hat{Z}(x)x\mathrm{J}_0(x)\mathrm{d}x,$$

$$2\pi\mu r_0 u(r,\, z,\, t)/P = \frac{1}{\xi}\int_0^{\infty}\left(\frac{1}{2\pi \mathrm{i}}\int_{c_0-\mathrm{i}\infty}^{c_0+\mathrm{i}\infty} u_0^{LH}\frac{\mathrm{e}^{\tau y}}{y}\mathrm{d}y\right)\hat{Z}(x)x\mathrm{J}_1(x)\mathrm{d}x, \tag{5}$$

where

$$w_0^{LH} = (\gamma_0 \mathrm{e}^{-\alpha_0\zeta/\xi} - 2x^2\mathrm{e}^{-\beta_0\zeta/\xi})\frac{\alpha_0}{\Delta_0},\quad u_0^{LH} = (\gamma_0 \mathrm{e}^{-\alpha_0\zeta/\xi} - 2\alpha_0\beta_0\mathrm{e}^{-\beta_0\zeta/\xi})\frac{x}{\Delta_0},$$

$$\alpha_0 = \sqrt{x^2 + (c_2^2/c_1^2)y^2},\quad \beta_0 = \sqrt{x^2+y^2},\quad \gamma_0 = 2x^2 + y^2,\quad \Delta_0 = \gamma_0^2 - 4\alpha_0\beta_0 x^2,$$

$$\zeta = \frac{z}{r_0},\quad \xi = \frac{r}{r_0},\quad \hat{Z}(x) = 2\frac{\mathrm{J}_1(x/\xi)}{x/\xi},\quad c_1 = \sqrt{\frac{\lambda+2\mu}{\rho}},\quad c_2 = \sqrt{\frac{\mu}{\rho}}.$$

Note that a nonstationary solution for $t \to \infty$ approaches a static solution, which can be presented in the following form:

$$2\pi\mu r_0 w_{st}(r,\, z)/P = \frac{1}{2\xi}\int_0^{\infty}\mathrm{e}^{-x\zeta/\xi}\left(\frac{x\zeta}{\xi} + 2(1-2\nu)\right)\hat{Z}(x)\mathrm{J}_0(x)\mathrm{d}x, \tag{6}$$

$$2\pi\mu r_0 u_{st}(r,\, z)/P = \frac{1}{2\xi}\int_0^{\infty}\left(\frac{x\zeta}{\xi} - (1-2\nu)\right)\hat{Z}(x)\mathrm{J}_1(x)\mathrm{d}x. \tag{7}$$

The Lamb's problem (a concentrated load) is related to representations (5)–(7), where $\hat{Z}(x) = 1$.

4. Numerical analysis

Taking into account positions of singular points of the integrated functions (branch points $\pm\mathrm{i}x$, $\pm\mathrm{i}(c_1/c_2)x$ and the poles $\pm\mathrm{i}(c_R/c_2)x$) the integration contour AB in the inverse Laplace transformation is replaced by the contour $CDEF$ consisting of the sectors DE, CD and EF(see Fig. 1), which is in agreement with the Cauchy's integral theorem.

For instance,

$$f(\tau) = \frac{1}{2\pi\mathrm{i}}\int_{c_0-\mathrm{i}\infty}^{c_0+\mathrm{i}\infty}\tilde{f}(y)\mathrm{e}^{y\tau}\mathrm{d}y = \mathrm{J}_1 + \mathrm{J}_2 + \mathrm{J}_3, \tag{8}$$

where: J_1 is the integral calculated along the sector DE, J_2 is the integral calculated along the sector CD, and J_3 is the integral calculated along the sector EF.

Taking into account the property of the transform $\tilde{f}(y)$ of the function $f(\tau)$, i.e., $\overline{\tilde{f}(y)} = \tilde{f}(\bar{y})$ (bar denotes a conjugated value), the integrals have the forms

$$\mathrm{J}_1 = \frac{1}{\pi}\mathrm{e}^{c_0 t}\int_0^{\beta}\big(\cos(\eta t)\mathrm{Re}(\tilde{f}(c_0+\mathrm{i}\eta)) - \sin(\eta t)\mathrm{Im}(\tilde{f}(c_0+\mathrm{i}\eta))\big)\mathrm{d}\eta, \tag{9}$$

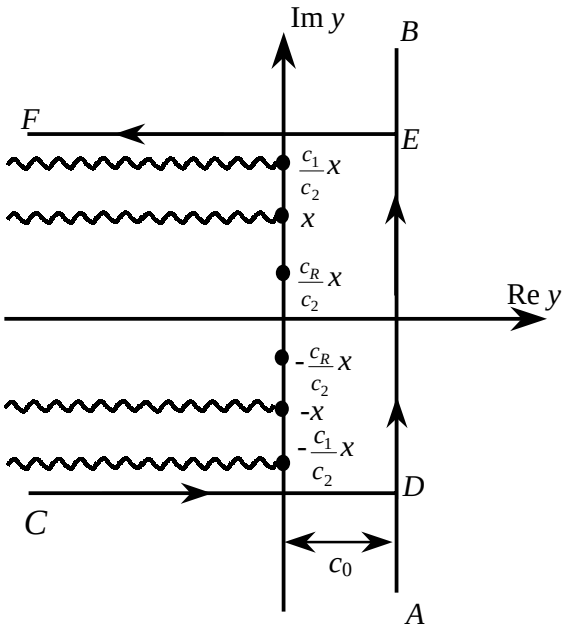

Fig. 1. Integration contour of the inverse Laplace transformation and singularities of the integrated functions.

$$J_2 = J_3 = -\frac{1}{2\pi}\int_{-\infty}^{c_0 t} e^{\eta}\left(\sin(\beta t)\mathrm{Re}(\tilde{f}(\frac{\eta}{t}+i\beta)) + \cos(\beta t)\mathrm{Im}(\tilde{f}(\frac{\eta}{t}+i\beta))\right)\frac{d\eta}{t}. \tag{10}$$

The numerical computations of integrals (9) and (10) are carried out using the results included in Ref. [8], and also applying the Gauss quadrature formula. During the numerical analysis of the inverse Hankel transforms the occurred integrals are replaced by a sum of finite integrals with the limits defined by the roots of the appropriate Bessel's function of the form

$$I = \int_0^{\infty} h(x)J_n(x)dx = \sum_{k=0}^{\infty} I^k, \quad I^k = \int_{x_{n,k}}^{x_{n,k+1}} h(x)J_n(x)dx \tag{11}$$

where $x_{n,k}$, $k = 1, 2, \ldots$ is the kth positive zero of $J_n(x)$, $x_{n,0} = 0$. $h(x)$ denotes under integral functions in Eqs. (5)–(7). The series in Eq. (11) is an alternating series, and the summation can be carried out using the ε-algorithm of Wynn [8]. In order to obtain numerically the integrals I^k the Gauss quadrature formula is applied.

In order to compare the obtained results with those known from literature and related to the Lamb's problem [5,6], the following parameters are taken: $\mu = \lambda$, $\nu = 0.25$.

The parameters, occurred in Eqs. (9) and (10), have the following values: $c_0 = 5/t$, $\beta = xc_1/c_2 + 5/t = \sqrt{3}x + 5/t$. The numerical analysis of the inverse Hankel and Laplace transforms is carried out using Eqs. (9) and (10). The obtained results are shown in Figs. 2–4.

In Fig. 2 the non-dimensional horizontal displacement in the radial direction versus non-dimensional time is reported. The results are presented for different values of the non-dimensional parameter $\xi = r/r_0$, where r_0 is the radius characterizing the load area. The dashed curve corresponds to the jump input of the type of concentrated force ($r/r_0 = \infty$), and both analytical

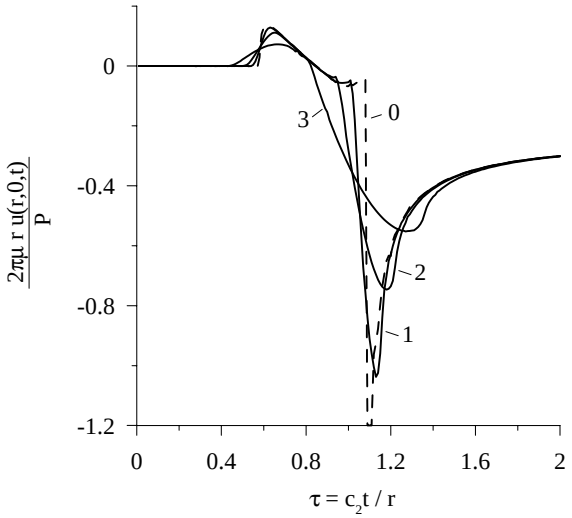

Fig. 2. Horizontal displacement versus non-dimensional time for different values of the radius r_0 characterizing the loaded area (dashed curve 0: $r/r_0 = \infty$, solid curves 1: $r/r_0 = 16$, 2: $r/r_0 = 8$, 3: $r/r_0 = 4$).

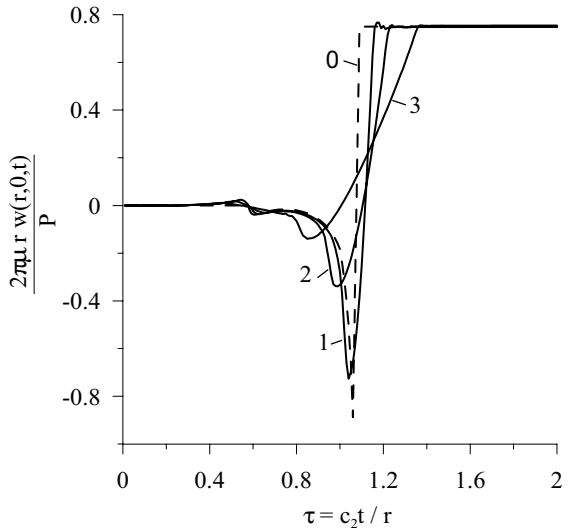

Fig. 3. Vertical displacement versus non-dimensional time for different r_0 values (dashed curve 0: $r/r_0 = \infty$, solid curves 1: $r/r_0 = 16$, 2: $r/r_0 = 8$, 3: $r/r_0 = 4$).

and numerical results concerning this load are reported in Ref. [5,6]. The solid curves correspond to the uniformely distributed load within the circle area of the radius r_0. Curve 1 ($\xi = r/r_0 = 16$) characterizes displacement of a point located in the distance of $16r_0$ from the load centre. Curves 2 (3) characterize displacements of the points located in the distances of $8r_0$ ($4r_0$) from the load centre, respectively.

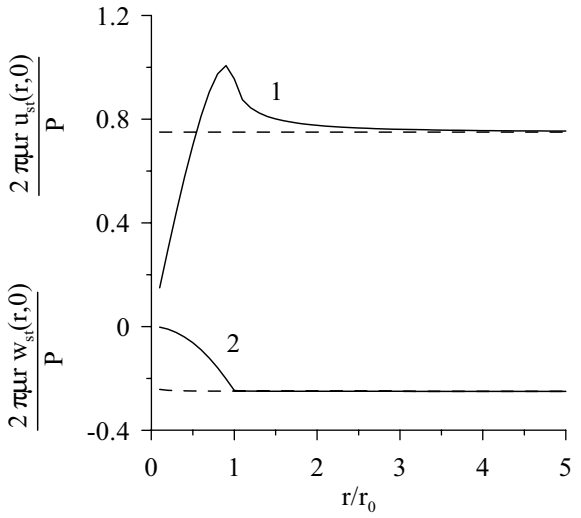

Fig. 4. Static solution for the dimensionless vertical displacements (curves 2) and dimensionless horizontal displacement (curves 1) versus r/r_0. (Dashed curves correspond to a concentrated force, solid curves are referred to a loaded area with the radius r_0).

Consider briefly the first case (concentrated force). A point located at a distance of r metres from the load origin is achieved by perturbation of the dilatation wave (P-wave) in the time instant r/c_1 (the corresponding non-dimensional time $\tau = c_2(r/c_1)/r = c_2/c_1 \approx 0.557$). In the time instant r/c_2(the non-dimensional time $\tau = c_2(r/c_2)/r = 1$) the observation point is reached by a distortion wave (S-wave) moving with the c_2 velocity. A Rayleigh wave reaches the observation point at the time instant r/c_R ($\tau = c_2/c_R = c_2/(c_2(\sqrt{2} - 2/\sqrt{3})) \approx 1.088$), and $c_R = 0.919\, c_2$. Both theoretical and numerical analysis of the problem [5,6] exhibits a singular perturbation yielded by the Rayleigh wave (both u and w become infinite). A nonstationary horizontal displacement after a certain time interval approaches a static solution, i.e. $(2\pi\pi r/P)u(r, 0, t) \to -(1 - 2v)/2 = -0.25$.

Consider now the uniformaly distributed load (see, for example, curve 3), and a point located in the instance of r metres from the load centre. A disturbance does not appear until the time instant of $(r - r_0)/c_1$. The observation point is reached by the P-wave moving with the velocity c_1 at the time instant $(r - r_0)/c_1$ ($\tau = (1 - r_0/r)c_2/c_1 = (3/4)\sqrt{3}/3 \approx 0.433$). The S-wave with velocity c_2 reaches the observation point at the time instant $(r - r_0)/c_2$ ($\tau = 1 - r_0/r = 3/4$). The observation point is achieved by the surface Rayleigh wave moving with the velocity $c_R = 0.919\, c_2$ in the time instant $(r - r_0)/c_R$ ($\tau = 0.75c_2/c_R \approx 0.816$). Note also that in the time instant $(r + r_0)/c_R$ ($\tau = 1.25c_2/c_R \approx 1.36$) the last perturbation yielded by the most distant loading point and moving with the velocity $c_R = 0.919\, c_2$ reaches the observation point. Comparing the curves 1, 2, 3 with the dashed curve 0 (solution to the ''Lamb's problem'') one may conclude, that after the Rayleigh surface wave transition caused by a disturbance occurred in a point of the loaded surface situated at the largest distance with respect to the analysed point, the Lamb's analytical solution can be used. In addition, the accuracy of the results yielded by the Lamb's formula increases with the increase of the distance between two mentioned points (see curve 1 in Fig. 2).

The vertical displacement at the surface point of the elastic half-space versus the non-dimensional time is reported in Fig. 3 for different $\xi = r/r_0$ values. The same description as in the case of Fig. 2 holds, and also the observed behaviour is similar. An unstationary vertical displacement for various disturbance areas, after a certain time interval approaches a static solution, i.e. $(2\pi\pi r/P)w(r,0,t)\to 1-v=0.75$.

Finally, in Fig. 4 the non-dimensional static horizontal displacements (curves 1) and vertical displacements (curves 2) versus parameter $\xi = r/r_0$ are reported. The dashed curves correspond to the concentrated force, whereas the solid curves refer to the uniformly distributed loaded area on the whole circle surface with the radius r_0. The obtained results do agree well with de Saint-Venant principle stating that on a certain distance (for example $r = 3r_0$) a solution with respect to the concentrated force is equal (with a certain accuracy) to a solution with respect to the loaded area defined by the radius r_0.

5. Conclusions

The carried out numerical analysis yields the following conclusion. The deformations appeared in the certain distance (for instance, on the length of three radiuses of the loaded area) from the load centre of various load distributions located in the plane being a boundary of an elastic half-space differ insignificantly after the Rayleigh wave transition takes place, and the analytical solution to the Lamb's problem can be used.

In other words, the de Saint-Venant principle can be used in various elastodynamical problems on a surface after the lapse of time $t = l/c_R$ (c_R is the Rayleigh wave velocity), where l denotes a largest distance between observed point and a point belonging to the loaded area, only if the reflected waves do not appear.

References

[1] S. Timoshenko, J.N. Goodier, Theory of Elasticity, McGraw-Hill, New York, 1951.
[2] W. Nowacki, Thermoelasticity, 2nd Edition, PWN–Pergamon Press, Warsaw, 1986.
[3] H. Lamb, On the propagation of tremors over the surface of an elastic solid, Philosoptical Transactions of the Royal Society of London Series A 203 (1904) 1–42.
[4] Y.C. Fung, Foundations of Solid Mechanics, Prentice-Hall, Englewood Cliffs, NJ, 1965.
[5] J.D. Achenbach, Wave Propagation in Elastic Solids, American Elsevier, New York, 1973.
[6] A.C. Eringen, E.S. Suhubi, Elastodynamics. Volume II. Linear Theory, Academic Press, New York, 1975.
[7] C.Y. Wang, J.D. Achenbach, Lamb's problem for solids of general anisotropy, Wave Motion 24 (1996) 227–242.
[8] R. Piessens, E. De Doneker-Kapenga, C.W. Überhuber, et al., QUADPACK: A Subroutine Package for Automatic Integration, Springer, Berlin, 1983.